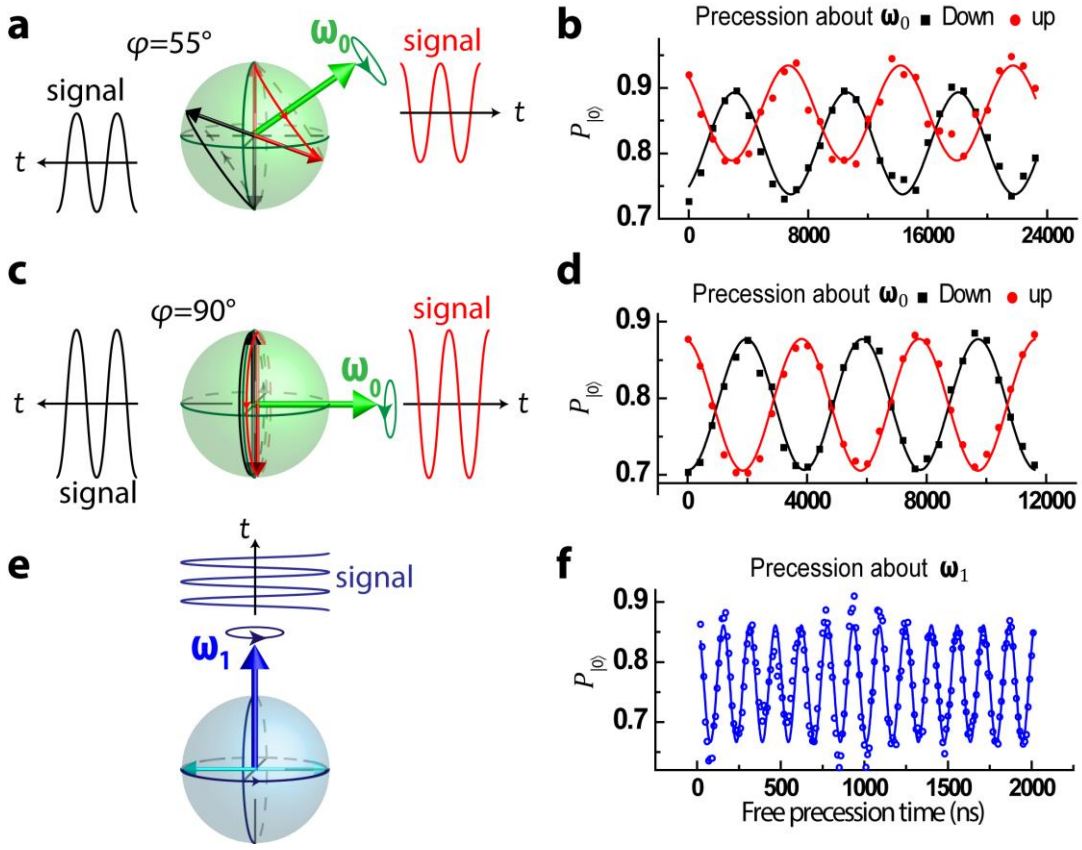

Supplementary Figure S1 | Characterization of the two-qubit system. a-d, When the nuclear spin is polarized along the $\boldsymbol{\omega}_1$ axis, its free precession signal about the $\boldsymbol{\omega}_0$ axis is modulated by the relative angle φ between the conditional local fields. **a-b,** When $\varphi < 90^\circ$, the centre lines of the free precession signals from the states $|\uparrow\rangle$ and $|\downarrow\rangle$ are offset from each other and the angle φ can be measured. The symbols are experimental data and the lines are fitting to a cosine function. **c-d,** When φ is tuned to be 90° by adjusting the orientation of the magnetic field, the centre lines of the free precession signals coincide. The strength ω_0 was measured to be $0.256(2)$ MHz by fitting the oscillation signal. **e-f,** When the nuclear spin is polarized along the $\boldsymbol{\omega}_0$ axis, its free precession about the $\boldsymbol{\omega}_1$ axis gives $\omega_1 = 6.410(2)$ MHz, in agreement with the pulsed optically detected magnetic resonance measurement.

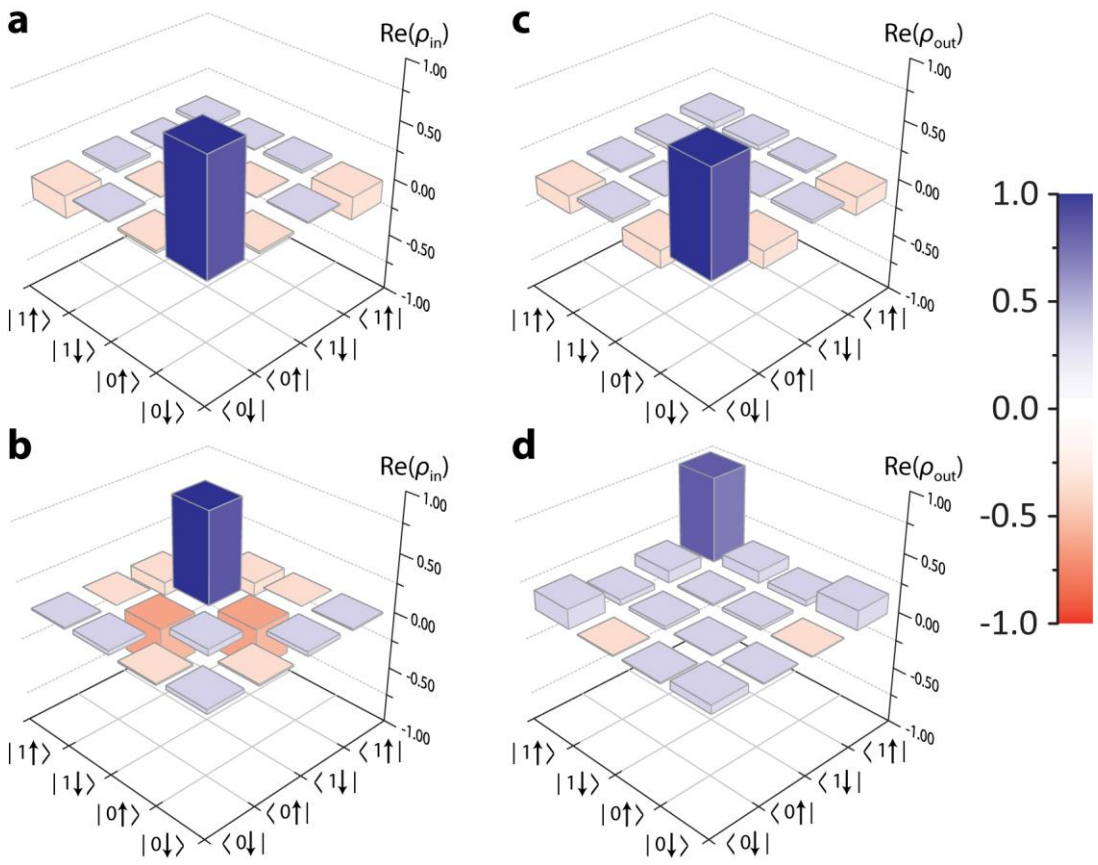

Supplementary Figure S2 | State tomography of the two qubits initially in a basis state. The system was prepared in two basis states and the state tomography was carried out before (**a** & **b**) and after (**c** & **d**) applying the designed controlled-NOT (C_eNOT_n) gate. The imaginary parts of the measured density matrices were negligible (not displayed). **a,** State tomography on the initial state $|0\downarrow\rangle$ with state fidelity of 0.98(1). **b,** State tomography on the initial state $|1\downarrow\rangle$ shows that the state is prepared with state fidelity of 0.89(2). **c,** State tomography on the resultant state after apply the gate on $|0\downarrow\rangle$ .The nuclear spin was left unchanged with a final state fidelity of 0.93(1). **d,** State tomography on the resultant state after applying the gate on $|1\downarrow\rangle$. The nuclear spin was flipped with a final state fidelity of 0.86(1).

Supplementary Table S1 | Timing parameters (in ns) of the DD sequences designed for realizing various two-qubit quantum gates. N is the number of pulses, and t_α denotes the interval between the pulses (note that the pulse sequences are symmetric so only the first halves of the DD sequences are listed).

a, Controlled-NOT gate (C_eNOT_n)

N	t_0	t_1	t_2	t_3	t_4	t_5	t_6	t_7
4	545.3	1013.0	467.8	-	-	-	-	-
6	543.7	1007.5	546.3	82.5	-	-	-	-
8	409.3	587.1	442.3	596.1	331.6	-	-	-
10	388.4	1008.6	399.6	121.0	381.0	39.4	-	-
12	383.9	395.9	327.1	447.6	332.7	407.3	207.1	-
14	234.3	212.9	311.4	277.7	293.9	203.7	171.0	316.3

b, Nuclear spin Hadamard gate (H_n)

N	t_0	t_1	t_2	t_3	t_4	t_5	t_6	t_7
4	474.6	804.9	330.4	-	-	-	-	-
6	316.5	335.5	333.5	314.6	-	-	-	-
8	328.3	354.4	300.5	455.2	180.8	-	-	-
10	183.8	349.8	162.9	158.6	234.2	72.6	-	-
12	169.4	337.0	168.0	163.7	182.7	155.1	135.7	-
14	163.0	170.3	162.0	165.9	159.7	163.3	168.7	154.0

c, Nuclear spin Pauli-X gate (X_n)

N	t_0	t_1	t_2	t_3	t_4	t_5	t_6	t_7
4	623.9	936.3	312.4	-	-	-	-	-
6	467.8	779.0	468.2	157.0	-	-	-	-
8	467.8	466.6	311.6	469.4	156.6	-	-	-
10	312.6	309.7	309.3	314.2	313.9	311.8	-	-
12	298.2	461.7	337.8	290.9	290.1	332.9	159.6	-
14	316.3	293.8	295.0	291.8	287.0	353.5	338.1	297.3

d, Nuclear spin Pauli-Z gate (Z_n)

N	t_0	t_1	t_2	t_3	t_4	t_5	t_6	t_7
4	234.6	351.1	116.5	-	-	-	-	-
6	211.1	233.8	216.9	194.3	-	-	-	-
8	153.8	212.6	159.3	215.4	114.9	-	-	-
10	104.2	177.0	103.9	119.7	143.2	54.5	-	-
12	82.6	110.1	93.5	114.8	122.0	126.7	53.6	-
14	68.2	78.0	68.2	78.0	68.3	78.0	68.3	39.0

e, Two-qubit NULL gate (NULL)

N	t_0	t_1	t_2	t_3	t_4	t_5	t_6	t_7
4	117.5	234.0	116.6	-	-	-	-	-
6	77.9	78.1	78.2	78.0	-	-	-	-
8	82.3	111.3	85.5	123.1	66.7	-	-	-
10	51.4	55.8	51.4	51.3	53.3	49.1	-	-
12	55.4	65.3	50.0	71.4	68.6	97.3	6.0	-
14	35.7	33.9	28.9	36.4	47.1	48.4	43.9	36.9

Supplementary Note 1: Theoretical description of the NV centre system

Pure-dephasing approximation

Here we discuss the pure-dephasing approximation for the NV centre system. We remark that such an approximation is not necessary for the design protocol to be applicable though it does simplify the numerical optimization in this work. In this subsection we use the magnetic number $m = 0, \pm 1$ to label the centre spin states.

We model the system by considering an NV centre coupled to the bath spins through hyperfine interaction. The bath consists of the ^{14}N host nuclear spin and ^{13}C nuclear spins with natural abundance of 1.1%. Under an external magnetic field $\mathbf{B} = B_z \hat{\mathbf{z}} + \mathbf{B}_\perp$, the system Hamiltonian can be written as

$$\mathcal{H} = \Delta (S^z)^2 - \gamma_{\mathrm{e}} \mathbf{B} \cdot \mathbf{S} - P^{(\mathrm{N})} (I^z_{(\mathrm{N})})^2 - \gamma^{(i)}_{\mathrm{n}} \mathbf{B} \cdot \mathbf{I}_{(i)} + \mathbf{S} \cdot \underline{\boldsymbol{\alpha}}^{(i)} \cdot \mathbf{I}_{(i)} + \mathbf{I}_{(i)} \cdot \underline{\boldsymbol{\beta}}^{(i>j)} \cdot \mathbf{I}_{(j)}, \quad \text{(S1)}$$

where $\hat{\mathbf{z}}$ is along the NV symmetry axis, $\Delta = 2.87$ GHz is the zero-field splitting of the NV centre spin, $\gamma_{\mathrm{e}} = 2.80$ MHz/G and $\gamma^{(i)}_{\mathrm{n}}$ are respectively the gyromagnetic ratios of the centre spin $\mathbf{S}$ and the ith nuclear spin $\mathbf{I}_{(i)}$ ($\gamma^{(i)}_{\mathrm{n}} = 1.07$ kHz/G for a ^{13}C nuclear spin, and $\gamma^{(\mathrm{N})}_{\mathrm{n}} = 0.31$ kHz/G for the nitrogen spin), $\underline{\boldsymbol{\alpha}}^{(i)}$ represents the hyperfine coupling between the electron spin and the ith nuclear spin, $\underline{\boldsymbol{\beta}}^{(i>j)}$ represents the dipolar interaction between the ith and jth bath spins, $P^{(\mathrm{N})} = -4.95$ MHz is the quadrupole moment of the ^{14}N spin, and summation over i and j is implied. Note that the subscript and superscript "(N)" is reserved to refer to the ^{14}N host nuclear spin.

When $\gamma_{\mathrm{e}} B_\perp$ and the hyperfine interaction strength $\left|\alpha^{(i)}\right|$ are both $\ll \left|\Delta \pm \gamma_{\mathrm{e}} B_z\right|$, the direct flipping of the NV centre spin between the $m = \pm 1$ states and the $m = 0$ state is suppressed by the large zero-field splitting Δ. Therefore, m is a good quantum number and perturbation treatment can be performed by separating the full system (i.e. centre spin + nuclear spins) Hamiltonian by

$$\begin{aligned}
\mathcal{H}^0 &= \Delta \left(S^z\right)^2 - \gamma_{\mathrm{e}} B_z S^z, \\
\mathcal{V} &= S^z \boldsymbol{\alpha}^{(i)}_z \cdot \mathbf{I}_{(i)} - \gamma^{(i)}_{\mathrm{n}} \mathbf{B} \cdot \mathbf{I}_{(i)} + P^{(\mathrm{N})} (I^z_{(\mathrm{N})})^2 + \mathbf{I}_{(i)} \cdot \underline{\boldsymbol{\beta}}^{(i>j)} \cdot \mathbf{I}_{(j)} \\
&\quad + \left(S^+ \left(-\gamma_{\mathrm{e}} \tilde{B}_\perp + \boldsymbol{\alpha}^{(i)}_\perp \cdot \mathbf{B}_{(i)} \right) + S^- \left(-\gamma_{\mathrm{e}} \tilde{B}^*_\perp + \boldsymbol{\alpha}^{(i)*}_\perp \cdot \mathbf{I}_{(i)} \right) \right) \\
&= \mathcal{V}^0 + S^+ \mathcal{V}^+ + S^- \mathcal{V}^-,
\end{aligned} \quad \text{(S2)}$$

where $\boldsymbol{\alpha}_\mu = \alpha_{\mu\nu} \hat{\mathbf{x}}^\nu$, $\tilde{B}_\perp = \dfrac{B_x - i B_y}{2}$, $\boldsymbol{\alpha}_\perp = \dfrac{\boldsymbol{\alpha}_x - i \boldsymbol{\alpha}_y}{2}$, $S^\pm = S^x \pm i S^y$, and $\mathcal{V}^0$, $\mathcal{V}^\pm$ are defined by comparing the corresponding terms. Clearly, the $m = 0, \pm 1$ centre spin eigenstates are all eigenstates of the unperturbed Hamiltonian, with eigenenergies given by $E_0 = 0$ and $E_{\pm 1} = \Delta \mp \gamma_{\mathrm{e}} B_z$.

Perturbation treatment, up to second order, gives the effective conditional Hamiltonian (acting on the nuclear spins)

$$h_m = \Delta m^2 - \gamma_{\rm e} B_z m + \mathcal{P}^m \left(\mathcal{V} + \mathcal{V} \frac{1-\mathcal{P}^m}{E_m - \mathcal{H}_0} \mathcal{V} \right) \mathcal{P}^m, \tag{S3}$$

where $\mathcal{P}^m = |m\rangle\langle m|$ is a projection operator. Evaluating, we have

$$\begin{aligned} h_{\pm 1} &= \Delta \mp \gamma_{\rm e} B_z \pm \boldsymbol{\alpha}_z^{(i)} \cdot \mathbf{I}_{(i)} - \gamma_{\rm n}^{(i)} \mathbf{B} \cdot \mathbf{I}_{(i)} + \mathbf{I}_{(i)} \cdot \underline{\boldsymbol{\beta}}^{(i>j)} \cdot \mathbf{I}_{(j)} + 2 \frac{\mathcal{V}^{\pm} \mathcal{V}^{\mp}}{E_{\pm 1}}, \\ h_0 &= -\gamma_{\rm n}^{(i)} \mathbf{B} \cdot \mathbf{I}_{(i)} + \mathbf{I}_{(i)} \cdot \underline{\boldsymbol{\beta}}^{(i>j)} \cdot \mathbf{I}_{(j)} - 2 \left(\frac{\mathcal{V}^{-} \mathcal{V}^{+}}{E_{+1}} + \frac{\mathcal{V}^{+} \mathcal{V}^{-}}{E_{-1}} \right). \end{aligned} \tag{S4}$$

Straightforward computation gives

$$\begin{aligned} h_m = E_m + C_m + \mathcal{C}_m^{(\rm N)} + P^{(\rm N)} (I_{(\rm N)}^z)^2 - \gamma_{\rm n}^{(i)} \mathbf{B} \cdot \mathbf{I}_{(i)} + \left(-\mathbf{B} \cdot \underline{\boldsymbol{\delta \mathbf{G}}}_m^{(i)} + \boldsymbol{\mathcal{A}}_m^{(i)} \right) \cdot \mathbf{I}_{(i)} \\ + \mathbf{I}_{(i)} \cdot (\underline{\boldsymbol{\beta}}^{(i>j)} + \underline{\boldsymbol{\delta \beta}}^{(i>j)}) \cdot \mathbf{I}_{(j)}, \end{aligned} \tag{S5}$$

with the second order corrections given by

$$\begin{aligned} C_{\pm 1} &= \frac{1}{E_{\pm 1}} \left(\gamma_{\rm e}^2 \frac{|B_x|^2 + |B_y|^2}{2} + \sum_{(i)} \frac{|\boldsymbol{\alpha}_x^{(i)}|^2 + |\boldsymbol{\alpha}_y^{(i)}|^2}{16} \right), \\ \mathcal{C}_{\pm 1}^{(\rm N)} &= \frac{1}{2E_{\pm 1}} \left(\sum_{\nu = x,y} |\boldsymbol{\alpha}_\nu^{(\rm N)}|^2 \, (I_{(\rm N)}^\nu)^2 \right), \\ \boldsymbol{\mathcal{A}}_{\pm 1}^{(i)} &= \pm \boldsymbol{\alpha}_z^{(i)} \mp \frac{\boldsymbol{\alpha}_x^{(i)} \times \boldsymbol{\alpha}_y^{(i)}}{2E_{\pm 1}}, \\ \underline{\boldsymbol{\delta \mathbf{G}}}_{\pm 1}^{(i)} &= \frac{\gamma_{\rm e}}{E_{\pm 1}} \begin{pmatrix} \alpha_{xx}^{(i)} & \alpha_{xy}^{(i)} & \alpha_{xz}^{(i)} \\ \alpha_{yx}^{(i)} & \alpha_{yy}^{(i)} & \alpha_{yz}^{(i)} \\ 0 & 0 & 0 \end{pmatrix}, \\ \underline{\boldsymbol{\delta \beta}}_{\pm 1}^{(i>j)} &= \frac{1}{E_{\pm 1}} \sum_{\mu = x,y} \boldsymbol{\alpha}_\mu^{(i)} \otimes' \boldsymbol{\alpha}_\mu^{(j)}, \\ \mathcal{O}_0 &= -\left(\mathcal{O}_{+1} + \mathcal{O}_{-1} \right) \quad \text{for} \quad \mathcal{O} = C, \mathcal{C}^{(\rm N)}, \boldsymbol{\mathcal{A}}^{(i)}, \underline{\boldsymbol{\delta \mathbf{G}}}^{(i)} \,\&\, \underline{\boldsymbol{\delta \beta}}^{(i)}, \end{aligned} \tag{S6}$$

where we have assumed $\underline{\boldsymbol{\alpha}}^{(\rm N)}$ to be diagonal[39], and $\otimes'$ here refers to the Kronecker product between vectors. We remark that $\underline{\boldsymbol{\delta \mathbf{G}}}^{(i)}$ is related to the enhanced *g*-tensor $\underline{\tilde{\mathbf{g}}}^{(i)}$ by $\underline{\tilde{\mathbf{g}}}^{(i)} = \underline{\mathbf{1}} + \underline{\boldsymbol{\delta \mathbf{G}}}^{(i)} / \gamma_{\rm n}^{(i)}$.

The essence of these conditional Hamiltonians is captured by writing generically in the form of $h_m = \mathcal{E}_m + \boldsymbol{\omega}_m^{(i)} \cdot \mathbf{I}_{(i)} + \mathbf{I}_{(i)} \cdot \underline{\tilde{\boldsymbol{\beta}}}^{(i>j)} \cdot \mathbf{I}_{(j)}$. Generally, the quantization axes of the nuclear spins ($\boldsymbol{\omega}_m^{(i)}$) depend on the state of the centre spin (m). Since $\gamma_{\rm e} |\alpha_{\mu\nu}^{(i)}| / (\gamma_{\rm n} \Delta)$ is of order 1 for a moderately strong hyperfine coupling, the enhancement of the *g*-tensor of the nuclear spin due to virtual flip-flops of the centre spin is significant when the magnetic field is not aligned along the NV symmetry axis[31,39]. This *g*-tensor enhancement, however, enters through $\boldsymbol{\omega}_0$ and $\boldsymbol{\omega}_{\pm 1}$ in reversed sign. This implies that under a general magnetic field the quantization axes $\boldsymbol{\omega}_m^{(i)}$ of a particular nuclear spin do not coincide. We also remark that $\mathbf{z}$ becomes a

well-defined quantization axis for the *i*th nuclear spin when $\mathbf{B} = B\mathbf{z}$ and $\underline{\boldsymbol{\alpha}}^{(i)}$ is almost diagonal, which are the conditions utilized in ref. 32.

Conditional evolution of the target nuclear spin

To illustrate the conditional evolution of the nuclear qubit, we restrict ourselves to the system formed only by the NV centre spin and the target ^{13}C spin (indexed by (*0*)). When the system is allowed to evolve freely, the system propagator within the pure-dephasing approximation is given by $U(t) = \sum_{m=0,1} \mathcal{P}^m \otimes \exp(-ih_m t)$, where for brevity we set $\hbar = 1$ throughout our treatment. In general $\hat{\boldsymbol{\omega}}_1^{(0)} \neq \pm\hat{\boldsymbol{\omega}}_0^{(0)}$ ($\hat{\boldsymbol{\omega}}_m^{(0)}$ denoting the unit vector along $\boldsymbol{\omega}_m^{(0)}$), so h_0 and $h_{\pm 1}$ do not commute, that is, the conditional nuclear spin evolution represents precession about different axes, which suffices to generate universal nuclear spin operators.

When the system is subjected to a series of centre spin π-pulses with timing intervals $\{t_\alpha\} \equiv \{t_\alpha \mid \alpha = 0,1,\ldots,N\}$, the system propagator is given by $U\{t_\alpha\} = \sum_{m=0,1} \mathcal{P}^m \otimes u_m\{t_\alpha\}$, where $u_0\{t_\alpha\} = e^{-ih_\sigma t_N} \ldots e^{-ih_1 t_1} e^{-ih_0 t_0}$ with $\sigma = 0$ or 1 for N being even or odd, and u_1 is similarly defined.

Supplementary Methods

Determination of $\boldsymbol{\omega}_0$ *and* $\boldsymbol{\omega}_1$

The conditional evolution of the nuclear qubit can be revealed by studying its free precession when the centre spin is prepared in different states. To be specific, we write $\boldsymbol{\omega}_0 = \omega_0\left(\sin\varphi\,\tilde{\mathbf{x}} + \cos\varphi\,\tilde{\mathbf{z}}\right)$ and $\boldsymbol{\omega}_1 = \omega_1\tilde{\mathbf{z}}$, and denote the spin operators for the nuclear qubit by I^{μ}. Note that in this notation $\tilde{\mathbf{x}} \neq \hat{\mathbf{x}}$ and $\tilde{\mathbf{z}} \neq \hat{\mathbf{z}}$ in general. To incorporate the effect of incomplete polarization, we suppose the nuclear qubit is initially represented by the density matrix ρ. We further denote the polarization of the target spin right after the polarization procedure by $\mathcal{M} = \mathrm{Tr}(I^{\tilde{z}}\rho) \in [-1/2, 1/2]$. When a high degree of polarization is achieved, i.e. $|\mathcal{M}| \approx 1/2$, the off diagonal elements of ρ has magnitude $\leq \sqrt{\frac{1}{4} - \mathcal{M}^2} \ll 1$, and so the contribution of the free precession signal due to the off-diagonal terms can be neglected. Therefore, the expectation value of $I_0^z(t)$ as a function of free evolution time t is given by

$$\langle I_0^z(t)\rangle \approx \mathcal{M}[\cos^2\varphi + \cos(\omega_0 t)\sin^2\varphi]. \qquad \text{(S7)}$$

Clearly the strength ω_0 is given by the frequency of the free precession signal. By comparing the corresponding signal with polarization along $|\uparrow\rangle$ and $|\downarrow\rangle$, the polarization $\mathcal{M}$ and the relative angle φ can be measured.

In Supplementary Fig. S1 we show the free precession signal when the magnetic field (fixed at 100 G) was orientated along different directions. Supplementary Figs. S1a-b show the scenario when $\mathbf{B}$ was aligned at $\sim 4^{\circ}$ from the NV symmetry axis. The angle φ was determined from the free precession signal in Supplementary Fig. S1b to be 55°. Supplementary Figs. S1c-d show the corresponding scenario when $\mathbf{B}$ was aligned at $\sim 13^{\circ}$ from the NV axis, which is the setting for the experimental results included in the main text. The symmetric oscillation about the common centre line of the precession signals indicates that φ was tuned to be 90°. A similar set of procedures would also reveal information of $\boldsymbol{\omega}_1$ (Supplementary Figs. S1e-f).

Numerical simulation of two-qubit gates

Regarding the two coupled spin-1/2's as a 4-level system, the average fidelity $\bar{F}$ of executing a unitary gate G by a system propagator $U\{t_\alpha\}$ can be simplified by[43]

$$\bar{F} = \int \mathrm{d}\Psi\ \mathrm{Tr}\left(U|\Psi\rangle\langle\Psi|U^{\dagger}G|\Psi\rangle\langle\Psi|G^{\dagger}\right) = \frac{\sum_j \mathrm{Tr}(UO_j^{\dagger}U^{\dagger}GO_jG^{\dagger}) + d}{d(d+1)}, \qquad \text{(S8)}$$

where $d = 4$ and $\{O_j\}$ is a complete orthonormal operator basis for the 4-level system satisfying $\mathrm{Tr}(O_j^{\dagger}O_k) = \delta_{jk}$. The DD sequences have the symmetric forms $\{t_0, t_1, \ldots, 2t_N, \ldots, t_1, t_0\}$ for $2N$ pulses and $\{t_0, t_1, \ldots, t_N, t_N, \ldots, t_1, t_0\}$ for $2N+1$ pulses.

We adopted a numerical maximization protocol based on a scheme similar to the one described in the GRAPE algorithm[50]. Starting with an initial guess of $\{t_\alpha\}_0$, in each maximization step we update $t_\alpha \to t_\alpha + \delta t_\alpha$ by $\delta t_\alpha = \epsilon \partial_{t_\alpha} \bar{F}$ such that $\delta \bar{F} \geq 0$, where $\epsilon > 0$ is a small numerical parameter. $\partial_{t_\alpha} \bar{F}$ can be calculated through the straightforward evaluation of $\partial_{t_\alpha} U$, which requires only the knowledge of the inter-qubit interaction but not the detailed spectrum of the bath.

As discussed in ref. 50, such an approach guarantees convergence only to local, but not global, maxima of $\bar{F}$. Besides, given resources of N π-pulses it is desirable to also minimize $\sum t_\alpha$ such that the coherence is better protected and the gate speed is faster. Therefore, one has to choose an appropriate initial guess $\{t_\alpha\}_0$ for a proper design of the DD gate sequence. In particular, we first surveyed a special subset of N-pulses sequences with the form $t_\alpha = t_{\mathrm{mod}(\alpha,2)}$, such that the parameter space is only two-dimensional. In addition, we restrict values of t_0 and t_1 such that the total gate operation time is reasonably short. The initial guess $\{t_\alpha\}_0$ is then determined by the values of t_0 and t_1 such that $\bar{F}$ attains a global maximum over this restricted two-dimensional parameter space. The DD gate sequence $\{t_\alpha\}_{\mathrm{DD}}$ is then found by numerical optimization of $\bar{F}$ in the larger parameter space.

We present in Supplementary Table S1 a comprehensive list of the designed DD gate sequences discussed in Fig. 2 of the main text.